The Role of Hydroxyl Groups in the Photophysics, Photostability, and (Opto)electronic Properties of the Fungi-derived Pigment Xylindein

Gregory Giesbers,[1] Taylor D. Krueger,[2] Jonathan D. B. Van Schenck,[1] Ryan Kim,[2] Ray Van Court,[3] Seri C. Robinson,[3] Christopher M. Beaudry,[2] Chong Fang,[2] Oksana Ostroverkhova[1*]

[1]Department of Physics, Oregon State University, Corvallis, Oregon 97331 United States

[2]Department of Chemistry, Oregon State University, Corvallis, Oregon 97331 United States

[3]Department of Wood Science and Engineering, Oregon State University, Corvallis, Oregon 97333 United States

ABSTRACT:

Organic semiconductors have attracted increasing attention due to their low cost, solution processability, and tunable properties. Of special interest are molecules with enhanced environmental stability. We have recently reported on (opto)electronic properties of a remarkably stable, naturally derived pigment xylindein. Here, we establish that one particular aspect of xylindein molecular structure, namely the presence of hydroxyl (OH) groups, is critical for enabling its enhanced stability and relatively high electron mobility. In particular, we synthesized a methylated derivative of xylindein, dimethylxylindein, where the OH groups are replaced with OCH_3 groups, and compared photophysics and (opto)electronic properties of dimethylxylindein

and xylindein. We reveal the presence of a long-lived excited state in dimethylxylindein, in contrast to xylindein, which has an efficient fast non-radiative pathway to the ground state. This results in significantly reduced photostability of dimethylxylindein as compared to xylindein. The effective electron mobility, obtained from space-charge-limited currents, in amorphous xylindein films was found to be four orders of magnitude higher than that in amorphous and crystalline dimethylxylindein films. In contrast, the photosensitivity of dimethylxylindein is about two orders of magnitude higher than that of xylindein. The mechanism of charge transport in all films was thermally-activated hopping, with the xylindein films characterized by considerably shallower charge traps than dimethylxylindein films, attributed to hydrogen bonding via hydroxyl groups promoting efficient conductive network in xylindein.

1. INTRODUCTION

Organic (opto)electronic materials have attracted considerable attention due to their low cost, enhanced processability, and tunable properties.[1] A variety of applications, including organic solar cells, light-emitting diodes, thin-film transistors (TFTs), sensors, and many others have been demonstrated.[2] One of the major issues for the wide-spread applications of organic materials is their relatively low stability with respect to exposure to environmental factors.[2] This issue drives a search for stable organic electronic materials and provides the motivation to understand how stability depends on the molecular structure and packing. In "conventional" organic semiconductors such as acene or thiophene derivatives, examples of molecular design strategies that resulted in enhanced stability of molecules in air include fluorination of the molecular core (e.g., in the case of fluorinated functionalized pentacene (Pn), hexacene, or anthradithiophene (ADT) derivatives as compared to their non-fluorinated counterparts[3–5]) and increasing the dimensionality of the molecule (e.g., in the case of bistetracene as compared to tetracene[6]). Additionally, over the past decade, hydrogen (H)-bonded pigments with "unconventional" molecular structures (exemplified by indigo, epindolidione, or quinacridone)[7–9] have been explored as organic (opto)electronic materials. These pigments exhibited enhanced photo and/or thermal stability in air, combined with relatively strong (opto)electronic performance,[7–10] both of which were partially attributable to the effects of intra- and intermolecular H-bonding. More generally, H-bonded organic materials are of interest for organic electronics[7–10] due to the potential to exploit H-bonds in inducing long-range molecular order,[8,10] which promotes charge carrier delocalization that could lead to enhanced electronic properties.

We recently reported on the optical and electronic properties of a highly stable pigment xylindein (Fig.1(a)), which is secreted by wood-staining fungi in the *Chlorociboria* genus.[11–13] Xylindein

belongs to a special class of external pigments produced by wood-decaying spalting fungi to defend the territory as they slowly grow and deeply penetrate into wood.[15] Because it can take years for the spalting fungi to fully colonize a log, the pigment they make must persist and not degrade in air under UV light, heat, and other environmental conditions. Xylindein has been used in art and intarsia since the 15th century, and its impressive color retention in these works of art in the present time is a testament to xylindein's environmental stability.[14,15] In terms of photostability in the presence of continuous illumination in air, xylindein considerably outperformed benchmark organic semiconductors TIPS-Pn and a relatively stable fluorinated ADT derivative diF TES-ADT.[11] The enhanced stability was accompanied by electron mobility of up to 0.4 $cm^2/(Vs)$ in amorphous xylindein films. However, how the enhanced stability and a relatively strong electronic performance of xylindein are determined by various aspects of its molecular structure, for example its peri-xanthenoxanthene (PXX) molecular core versus the presence of the hydroxyl (OH) groups (Fig. 1a) and H-bonding they enable, has not been established and is explored in the present paper.

The photophysical and (opto)electronic properties of molecules with the PXX core have been considerably less studied than those of benchmark organic semiconductors such as acene derivatives. For instance, photophysics of PXX and a small subset of its derivatives was characterized in detail only in the past three years.[16–18] The unsubstituted PXX exhibits optical

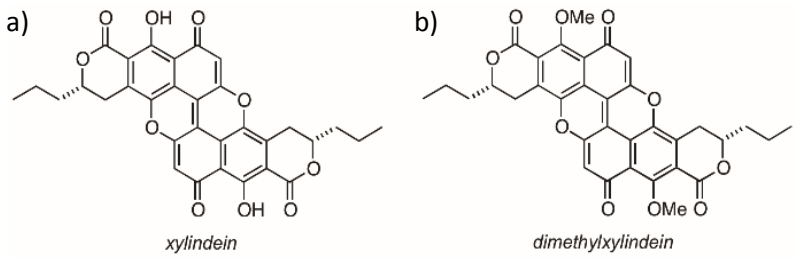

Figure 1. Molecular structure of xylindein (a) and dimethylxylindein (b).

absorption (fluorescence) maximum at ~440 nm (450 nm), fluorescence quantum yields (QYs) of 0.5–0.97 depending on the solvent, and solvent-dependent lifetimes of ~5–8 ns.[16] The functionalized PXX derivatives exhibited enhanced stability in air as compared to their parent carbon-based compound anthanthrene (which was attributed to the reaction-active site passivation due to heteroatoms/substituents on the molecular core) and compared to Pn; the enhanced stability was accompanied by TFT hole mobilities of up to 0.8 $cm^2/(Vs)$.[19] Because the unsubstituted PXX produced poor film morphology, several PXX derivatives featuring various solid-state packing motifs were synthesized and characterized in TFTs, exhibiting hole mobilities in the 0.04–0.9 $cm^2/(Vs)$ range.[19,20] Although predicted theoretically,[21] n-type behavior has not been experimentally observed in functionalized PXX derivatives.

The photophysical and electronic properties of xylindein are distinctly different from those of unsubstituted PXX and its derivatives studied in the literature.[16–20] For example, xylindein is non-fluorescent (QY < 0.1%), and it favors electron (n-type) transport. Therefore, in order to better understand properties of xylindein and relate them to the specifics of its molecular structure, we sought a molecule with a structure closer to that of xylindein as compared to PXX. In particular, we synthesized a methylated derivative of xylindein (dimethylxylindein, Fig. 1b), which has most of the features of xylindein's molecular structure (Figs. 1a and S1) except for the OH groups that are substituted with OCH_3 (OMe) groups. We performed a side-by-side comparison of optical and (opto)electronic properties of these two compounds, revealing dramatic differences in their photophysics and (photo)conductivity. In particular, we demonstrated that the processes enabled by the OH groups in xylindein are critical for its remarkable photostability and enhanced electronic properties.

2. MATERIALS AND METHODS

2.1. Extraction of xylindein

Xylindein was extracted in accordance with procedures detailed in our previous publications from both wild and lab grown sources.[11–13] Briefly, wild type xylindein was harvested from wood collected at Tidewater, Oregon, USA. The wood was identified from the characteristic blue-green color unique to *Chlorociboria* species. DNA extraction followed by Sanger sequencing of the internal transcribed spacer region and GenBank Megablast comparison identified the species responsible for staining the wood as *Chlorociboria aeruginosa.*[11] Lab grown xylindein was produced by *C. aeruginosa* (strain UAMH 11657) cultures maintained on 2% malt agar plates. These cultures were used to inoculate multiple 250 mL borosilicate mason jars each containing 50 mL of sterile 2% malt agar liquid media, which were then shaken at 99 rpm (Orbital Gene™ Scientific Industries) during growth. Mature colonies were collected and xylindein was extracted with a liquid-liquid dichloromethane (DCM)-water extraction, after blending to break apart cell walls with an Oster classic series blender. Extracted xylindein was then evaporated from DCM solution and rinsed multiple times with ethanol to remove contaminants.[13]

2.2.Synthesis of dimethylxylindein

Dimethylxylindein was prepared by diazomethane-mediated methylation of xylindein following the method of Hashimoto.[22]

2.3.Sample preparation

For optical measurements, xylindein or dimethylxylindein powder was dissolved into DCM or toluene at various concentrations ranging from 10^{-5} M – 10^{-2} M.

Xylindein films were cast from solutions in either DCM or CB at a concentration of 5 mg/ml. Pristine polycrystalline films of dimethylxylindein were cast from a 20 mg/ml solution in DCM. To create more homogeneous films and inhibit crystal formation, dimethylxylindein was mixed

with PMMA (Aldrich M_w=75,000) at a 4:1 weight ratio, and dissolved in DCM at an overall concentration of 20 mg/ml.

Films were prepared by drop-casting onto glass substrates, with patterned, treated Au electrodes for electrical measurements. Electrodes were patterned using conventional lift off photolithography, with thermally evaporated Au (80 nm) with a 10 nm Cr adhesion layer. Au electrodes were treated with polyethylenimine, ethoxylated (PEIE) to form a ~10 nm interlayer for work function reduction according to the procedures of Zhou et al.[23] Both coplanar and interdigitated electrode geometries, described in our previous publications,[24,29] were used.

For measurements of electronic properties in the sandwich geometry, xylindein:PMMA and dimethylxylindein:PMMA films at 1:1 and 1:2 weight ratios were prepared on Al (200 nm)/glass substrates followed by thermal deposition of another 200-nm Al layer patterned with a shadow mask.

2.4. Measurements of optical properties

Optical absorption spectra were measured using a tungsten-halogen lamp (LS-1, Ocean Optics) and a fiber-coupled Ocean Optics USB2000 spectrometer. Absorbance (A) was calculated from the incident (I_0) and transmitted (I) beam intensities as $A=-\log(I/I_0)$. Reflection losses were taken into account by referencing with respect to a cuvette with pure DCM. PL spectra were obtained using a cw 532 nm laser (Nd:YVO_4 from Coherent, Inc.) or a 633 nm He-Ne laser. For solution PL, light was collected using a parabolic mirror and detected with a fiber-coupled spectrometer (Ocean Optics USB2000-FLG). Film absorption and PL were measured on an inverted microscope (Olympus IX-71) with a 10× objective, fiber-coupled to a spectrometer. As a reference material for the PL quantum yield estimates of dimethylxylindein and xylindein, previously studied functionalized pentacene (Pn) derivative TIPS-Pn with QY = 0.75 in toluene,[24] was used.

Fluorescence lifetime measurements were performed using a 532 nm frequency-doubled Nd:YAG laser (HE-1060, Fianium, Inc.) with a repetition rate of 0.5 MHz as the excitation source. A single-photon avalanche photodiode (SPAD, Molecular Photonic Devices) was used in conjunction with a time-correlated single-photon counter (TCSPC) data analysis board (PicoQuant TimeHarp 200) for detection.

2.5. Femtosecond transient absorption (fs-TA) spectroscopy

The experimental set up for fs-TA spectroscopy has been described in detail previously.[25,26] In brief, we used a Ti:sapphire regenerative laser amplifier (Legend Elite-USP-1K-HE, Coherent, Inc.) with fundamental output laser pulses at ~800 nm center wavelength, ~35 fs pulse duration, ~3.7 W average power, and 1 kHz repetition rate. Second harmonic generation of a fraction of the 800 nm fundamental pulse in a 0.3-mm-thick Type-I BBO crystal produced the 400 nm actinic pump in the fs-TA experiments of xylindein and dimethylxylindein. In both experiments, the pump power was attenuated to ~0.2 mW. To achieve a longer detection time window that extends to ~4 ns, a quadruple-pass setup (with two UBBR2.5-2S broadband hollow retroreflectors, Newport, Inc.) was installed to effectively quadruple the delay line distance (NRT150, Thorlabs, Inc.) and the time delay controllable between the pump and probe interactions with the sample. Regarding the probe pulse, a portion of the laser fundamental output was focused onto a 2-mm-thick quartz cuvette filled with deionized water to generate supercontinuum white light (SCWL) without further temporal compression, so the probe pulse duration was on the ~150 fs range.[27,28] The transmitted probe beam (with a small crossing angle with the pump beam that was blocked past the sample) was dispersed in a spectrograph (Acton SpectraPro SP-2356, 300 mm focal length, Princeton Instruments) with a 300 grooves/mm, 500 nm blaze wavelength reflective grating before being imaged onto a front-illuminated Lumogen UV-coated CCD array camera (PIXIS:100F,

Princeton Instruments), which was synchronized with the main laser repetition clock. Spectral data were processed and stored by a customized LabVIEW suite before further analysis using the IGOR Pro 6.2 software (WaveMetrics, Inc.). Sample concentration for fs-TA experiments on xylindein and dimethylxylindein was made to reach the absorbance OD≈0.3 per mm at 400 nm. The steady-state UV/Visible spectra were taken before and after each time-resolved fs-TA experiment to check and ensure sample integrity under light irradiation conditions used in our studies at room temperature.

2.6. Measurements of photostability

For measurements of photostability, 10 μM solutions of xylindein and dimethylxylindein were prepared, and their optical absorption measured. The spectra were integrated in the S_0-S_1 absorption region (600–700 nm for xylindein, 520–590 nm for dimethylxylindein) yielding a data point at time t = 0. The solutions in vials sealed with a paraffin film to prevent solvent evaporation were then placed under the fume hood lights, in air, and spectral measurements were repeated at various time intervals. The S_0-S_1 spectra were integrated and the result normalized by that at t = 0. The experiment was carried out up to 3 weeks. For accelerated photobleaching testing, 10 μM solutions were placed in front of a solar simulator (Oriel 96000 with an AM 1.5G filter) with an aluminum foil lined encasement in order to increase the uniformity and total power of the light hitting the samples. Total irradiance was roughly 100 mW/cm^2, similar to the irradiance from the sun on a clear day. Absorbance was measured every 30 minutes over the course of 5.5 hours.

2.7.Measurements of (opto)electronic characteristics

For measurements of current-voltage characteristics, voltage was applied to the samples using a Keithley 237 source-measure unit and current in the dark was measured as a function of applied voltage ranging from 0–300 V.

Continuous-wave (cw) photocurrents in films were measured under 100 mW/cm^2 532 nm (Nd:YVO_4, Coherent, Inc.) or 633 nm (HeNe) photoexcitation. For ac photocurrent measurements, the light beam was chopped using an optical chopper at 100 Hz. A dc voltage of 100 V was applied to the samples consisting of films deposited on PEIE-treated Au interdigitated electrodes with a 25 μm gap using a Keithley 237 source-measure unit. For dc photocurrent measurements, the time evolution of the total current under the continuous light excitation (which was turned on and, after 20 s, turned off with shutter) was measured using the Keithley 237 source-measure unit and the photocurrent was calculated as the difference between the total and the dark current. For ac photocurrent measurements, the photoresponse from the sample was measured using a Stanford Research Systems (SRS830) lock-in amplifier as the voltage over a 10 kΩ resistor.

2.8. Measurements of temperature dependence

For temperature-dependent measurements, films deposited on PEIE-treated Au interdigitated electrodes with a 25 μm gap were incorporated in an optical cryostat (Janis STC-500), and temperature was controlled and measured with a PID temperature controller (Lakeshore model 335). Dark current and photocurrent measurements were carried out at 100 V in vacuum in the temperature range of 300–400 K with air as a coolant. Temperature-dependent photoluminescence measurements were taken from films deposited on glass substrates in the same manner except with liquid nitrogen as a coolant and in the temperature range of 100–300 K.

2.9. Density Functional Theory (DFT) calculations

The geometric structure and frontier orbital energies (Table 1) were calculated by Density Functional Theory using the Gaussian 16 software suite with the details described in our previous publication.[11] Briefly, the geometric structure was optimized with the B3LYP function and 6-311G++(d,p) basis set along with a polarizable continuum model for DCM to simulate the solvent

environment. Additionally, energies for the first excited states were calculated using time-dependent DFT in the ground state geometry; vertical transition energies are shown in Table 1. The triplet energies and molecular orbital energies for both xylindein and dimethylxylindein were also calculated using DFT methods (Table 1). An unrestricted B3LYP functional with the 6-311G++(d,p) basis set together with a polarizable continuum model for DCM was used to optimize the geometric configuration of both molecules.

3. RESULTS AND DISCUSSION

3.1. Photophysics in solution

Optical absorption and photoluminescence (PL) spectra of xylindein and dimethylxylindein in dichloromethane (DCM) are shown in Fig. 2. The absorption spectrum of xylindein exhibits a structure that is well described by two vibronic progressions, with the energies of 0-0 transitions offset by 0.06 eV (at 1.84 and 1.90 eV, or 674 nm and 654 nm) and vibrational energies of 0.13 eV and 0.16 eV (Table S1).[11] The presence of two vibronic progressions was previously attributed to the contribution of two xylindein tautomers, arising from different orientations of OH groups (Fig. S2), at a 70:30 ratio.[11] In support of this finding, the absorption spectrum of dimethylxylindein, which lacks OH groups, exhibits a single vibronic progression with the 0-0 energy at 2.17 eV (~571 nm) and vibrational energy of 0.18 eV (Fig. S3a and Table S1). Vibrational energies observed in xylindein and dimethylxylindein are comparable to those observed in a wide variety

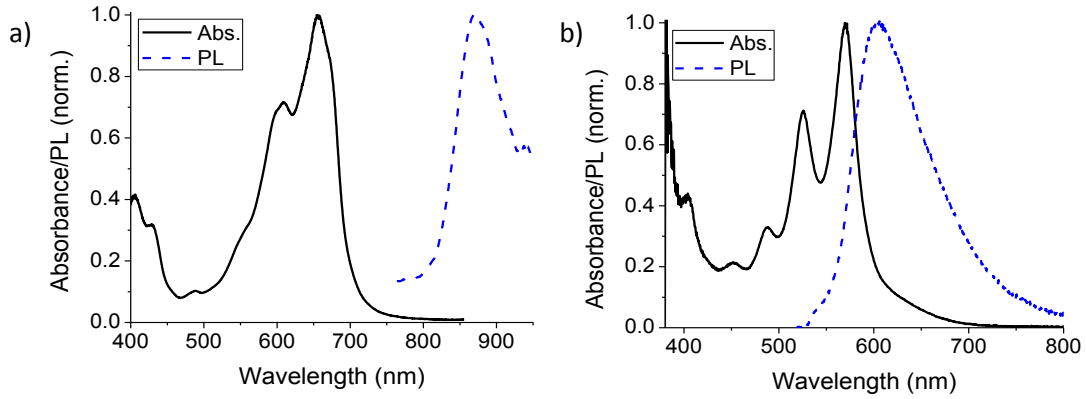

Figure 2. (a) Optical absorption and photoluminescence (PL) spectra of a dilute solution of (a) xylindein and (b) dimethylxylindein in dichloromethane (DCM). In xylindein (dimethylxylindein), PL was measured with a 633 nm (532 nm) excitation source.

of conjugated molecules in which the dominant coupling occurs to a C–C/C=C stretching mode.[16,21,29,30] This is most likely the case for molecules under current study, although other vibrational modes in the 0.13–0.2 eV range, previously identified in PXX derivatives,[21] could also contribute.

The PL emission in both xylindein and dimethylxylindein was weak, with the PL QYs of below 0.1% and 0.7%, respectively, in dilute DCM solutions. The dominant PL emission of xylindein, which peaks at ~870 nm in solution (Fig. 2a), has a large Stokes shift of 0.45 eV (~211 nm) and a lifetime of below~200 ps, limited by the time resolution of our PL measurements (Fig. S4 and Table S2). This observation is consistent with results from transient absorption spectroscopy with a near-infrared probe in xylindein solutions that revealed an ultrafast excited-state *intramolecular* proton transfer (ESIPT) from the OH group to the neighboring carbonyl group (both OH groups in the xylindein molecular framework participate in the ESIPT process that is further supported by quantum calculations), which enables a large Stokes shift to occur on sub-picosecond time scales within the electronic excited state. These findings with a focus on ultrafast spectroscopy and photophysics will be reported in detail in a separate publication.[31] Notably, the ESIPT process is

nontrivial for understanding the efficient energy dissipation upon photoexcitation and the excellent (photo)stability of xylindein in the condensed phase. While the ESIPT could be considered to occur with hydroxyl groups, there was limited experimental evidence to support it and its role in (photo)conductivity, which is the focus of our current work.

In contrast to xylindein, the Stokes shift in dimethylxylindein, wherein no ESIPT can occur, was considerably smaller at ~0.12 eV (~35 nm), which is comparable to a variety of PXX derivatives.[17,20] The PL emission of dimethylxylindein could be described by a vibronic progression with the 0-0 energy at 2.07 eV (~598 nm) and vibrational energy of 0.12 eV (Fig. S3b and Table S1). The vibronic peaks were more than a factor of two broader in the PL spectra of dimethylxylindein as compared to the absorption spectra. This trend is also common in PXX derivatives, which is indicative of differences in conformations and local environment experienced by the molecules in the ground and excited states. The dominant PL lifetime in dimethylxylindein was 250 ps, longer than that of xylindein (Fig. S4 and Table S2) but considerably shorter than typical lifetimes of previously studied PXX derivatives.[16]

A rather low PL QY of dimethylxylindein, at 0.7%, although higher than that of xylindein (<0.1%), is interesting, considering that a variety of PXX derivatives with Stokes shifts and other features of the optical spectra similar to those of dimethylxylindein exhibit QYs of >30%.[17] In order to gain insights into this observation, the excited state dynamics of these molecules was further investigated in ultrafast spectroscopy experiments, results of which for xylindein and dimethylxylindein in DCM solution are shown in Fig 3.

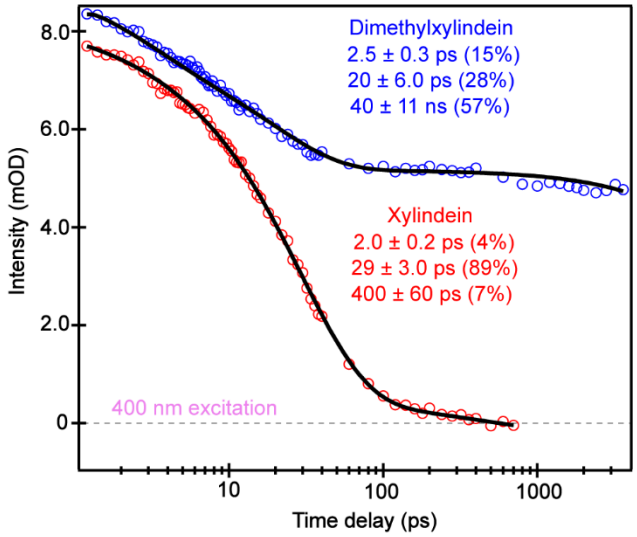

Figure 3. Ultrafast transient absorption obtained at 400 nm excitation as a function of pump-probe time delay for xylindein and dimethylxylindein in DCM, with associated decay rates and relative weights from the least-squares fits. The gray dashed line denotes the zero change of absorbance.

Following 400 nm excitation, we tracked the excited state absorption band from 515–520 nm for xylindein and from 465–470 nm for dimethylxylindein. The 400-nm actinic pump at the blue side of the S_0-S_1 electronic absorption populates higher-lying excited electronic states. We explored multiple actinic pump wavelengths and observed similar transient absorption dynamics, which infer an efficient $S_n \rightarrow S_1$ relaxation so we could focus on the decay dynamics of S_1. Both xylindein and dimethylxylindein exhibit a short (~2 ps) lifetime component accounting for ~4% and 15%, respectively, of the overall excited state relaxation, due to ultrafast solvation in the DCM environment. Both molecules also share a notable ~20–30 ps component, though this component is much more dominant in xylindein (~89%) than dimethylxylindein (~28%). The prevalence of this component in both cases rules out the possibility of *intermolecular* proton transfer as the mechanism of this relaxation, since dimethylxylindein has no dissociable protons, therefore it more likely involves characteristic conformational motions on the tens of ps time scale.[32,33] Conformational changes in the unsubstituted PXX have been previously observed;[16] therein, they manifested into dependence of the Huang-Rhys factor and wavelength of emission maximum on

the temperature and dependence of the excited state lifetime on solvent viscosity. For example, the thermally-activated conformational change with an activation energy of ~25–50 meV was inferred from the temperature dependence of PL spectral properties in solution. In xylindein and dimethylxylindein, the effect of conformational changes on the excited states dynamics is more dramatic, although the exact nature of the changes remains a research subject. Nevertheless, for any conformational change, the associated relaxation mechanism (responsible for the 20–30 ps lifetime) is non-radiative, and it may facilitate the molecule's approach to the S_1/S_0 conical intersection. Based on the relative contribution of this component to the overall excited state dynamics, this process is much more efficient in xylindein as compared to dimethylxylindein, and it could be responsible for the much lower PL QY in xylindein. For corroboration, we observed that the ground state bleaching (GSB) band (selected from 655–660 nm probe region) recovers with time constants of 36 ps (94%) and 300 ps (6%) in xylindein, largely matching its ESA band decay (red points in Fig. 3). Finally, there is a minor (7%) component with a ~400 ps lifetime in xylindein which may have a contribution from radiative relaxation manifested through the weak PL of this compound (Fig. 2a). No long-lived states were observed in xylindein (Figs. 3 and S4), confirming efficient deactivation of the excited state population in this molecule. We note that the matching ESA decay and GSB recovery of xylindein with a dominant ~30 ps time constant supports a nonradiative return directly from S_1 to S_0.

In contrast, dimethylxylindein exhibits a dominant (57% of the overall dynamics) long-lived state with a lifetime of ~40 ns (Fig. 3). This value represents a lower bound on the true lifetime of the long-lived state, as the exact determination is limited by our detection time span (~4 ns) of transient absorption experiments. Therefore, the true lifetime is most likely longer. The recovery of the negative GSB band of dimethylxylindein is difficult to analyze at early times due to spectral

Table 1. Properties of molecules in solution

	HOMO[1] (eV)	LUMO [1] (eV)	E_g[1] (eV)	S_1 [1] (eV)	T_1 [1] (eV)	Abs Max, [2] nm (eV)	PL Max, [2] nm (eV)	Stokes Shift, [3] nm (eV)	PLQY[4]
Xylindein	**– 6.49; – 6.30**	**– 4.31; – 3.99**	**2.18; 2.31**	**1.89; 1.93**	**1.03**	**674, 654 (1.84; 1.90)**	**870 (1.43)**	**211 (0.45)**	**<0.1%**
Dimethyl xylindein	**– 6.35**	**– 3.89**	**2.46**	**2.14**	**1.18**	**571 (2.17)**	**606 (2.05)**	**35 (0.12)**	**0.7%**

[1]Calculated using DFT, as described in Methods. The two reported values are from xylindein tautomers A and B (Fig. S2). For T_1, only the tautomer A energy is included. [2]Wavelength (energy) of the absorption or PL peak maximum in DCM; xylindein absorption maxima for the two tautomers were extracted from fits of the absorption spectrum to two vibronic progressions as discussed in Ref. [11]. [3]Calculated as a difference between the optical absorption and PL maxima in dilute DCM solution; in the case of xylindein, the absorption maximum (659 nm, Fig. 2a), with contribution from both tautomers, in DCM is used. [4]Measured in DCM as described in Methods.

overlap with the positive ESA band; however, the GSB band never fully recovers and we could fit it with a lifetime of 122 ns, corroborating the aforementioned ESA band decay dynamics (blue points in Fig. 3). The dominant presence of such a lingering component in dimethylxylindein implies the efficient formation of a dark state, which is consistent with our PL data showing no emission with a long lifetime (Fig. S4). Similar to the excited state deactivation via a conical intersection, the dark state formation would also contribute to the PL quenching and resulting low PL QY in this compound (Table 1). Additionally, it has important implications for the photostability as discussed below.

3.2. Photostability

Xylindein has been known to have remarkable photostability.[11]For example, our accelerated photobleaching testing of xylindein and a well-known pigment indigo (whose enhanced photostability has been attributed to ESIPT-promoted fast deactivation of the excited state[34]) demonstrated superior stability of xylindein over indigo (Figs. S5 and S6, which also include accelerated photobleaching testing data for another ESIPT pigment alizarin[35]). Elucidation of features of the xylindein molecular structure and photophysics responsible for its enhanced

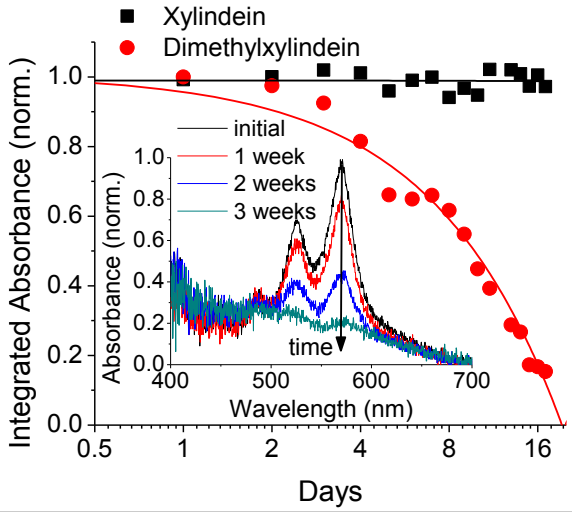

Figure 4. Integrated absorption spectra of xylindein and dimethylxylindein solutions in DCM versus time during exposure to white light in air. Trend lines are added to guide the eye. Inset shows dimethylxylindein absorption spectra at periodic intervals as the compound degrades upon exposure to light.

photostability is thus one of the motivations for the present work. Figure 4 shows integrated absorption over the S_0-S_1 transition for xylindein (600–700 nm) and dimethylxylindein (520–590 nm) in solution under continuous white light exposure in air. Notably, dimethylxylindein degraded substantially after only two weeks of exposure, while xylindein showed no evidence of photodegradation under identical illumination conditions. The latter consistent with our previous studies[11] in which xylindein lasted 25 weeks under the same illumination conditions before showing any signs of photodegradation, whereas TIPS-Pn decomposed within just three days. Similar trends for xylindein vs dimethylxylindein stability were observed under accelerated photobleaching testing conditions (Figs. S5 and S6). Significant photodegradation was also observed in deprotonated xylindein (Fig. S7), further demonstrating the importance of the hydroxyl group to the photostability of the molecule. The stark difference between the stability of xylindein and dimethylxylindein molecules can be related to the dramatic differences in their excited state dynamics revealed by transient absorption spectroscopy discussed above (Fig. 3). The dominant ~30 ps nonradiative deactivation of the excited-state xylindein prevents efficient

interaction of this molecule with oxygen, thus extending its lifespan. In contrast, dominant formation of a long-lived dark state in dimethylxylindein could facilitate interactions with oxygen, thus promoting formation of reactive oxygen species and consequent destruction of the parent molecule. We hypothesize that the dark state is a triplet state (T_1) and an effective degradation pathway is facilitated by energy transfer from the triplet state of dimethylxylindein to the ground-state triplet oxygen. Such energy transfer would be enabled by the triplet energy of dimethylxylindein (1.18 eV, Table 1) that is higher than 0.98 eV necessary to generate the reactive singlet oxygen species.[5,36]

3.3. Optical absorption and photoluminescence: films

Thin films of xylindein are amorphous, and no evidence of crystallization was observed regardless of film deposition conditions or processing. This is consistent with previous work:[27] although xylindein did crystallize when processed from hot phenol, solvent molecules were incorporated in the crystal structure; the attempts for their removal resulted in crystal collapsing, yielding an amorphous solid instead. In contrast, dimethylxylindein was prone to forming microscopic crystals, and so pristine dimethylxylindein films had both an amorphous and a crystalline phase as confirmed by XRD (Fig. S8). The two phases coexisted and the film morphology depended on deposition conditions; however, even in the best samples, crystallites were small and randomly oriented, resulting in rough disordered films, an observation similar to literature on unsubstituted PXX.[19] Our previous work with xylindein showed that 4:1 blends of xylindein with PMMA exhibited optical and electronic properties comparable with those of pristine xylindein, but had an improved film morphology and processability.[12] The same strategy was applied here to prevent crystallization and create more homogeneous dimethylxylindein films, thus 4:1 blends of dimethylxylindein:PMMA were investigated in addition to pristine

dimethylxylindein films. In the discussion below, these films, with a minimized formation of the crystalline phase, will be referred to as "amorphous". Pristine dimethylxylindein films which had both amorphous and crystalline regions will be referred to as "crystalline".

Figure 5 shows optical absorption and PL emission spectra for pristine xylindein, dimethylxylindein:PMMA, and pristine dimethylxylindein films. All absorption spectra exhibit a redshift Δ (see Table 2) in film with respect to those in solution, as well as peak broadening. These features have been previously attributed to enhanced intermolecular interactions in the film.[24,36] Amorphous xylindein film shows a larger Δ of ~110 meV (42 nm) as compared to ~70 meV (20 nm) in amorphous dimethylxylindein:PMMA film, but lower than ~240 meV (72 nm) in the crystalline pristine dimethylxylindein film (Fig. 5b). Varying solution-solid redshifts Δ have been previously observed in films of varying morphology and crystallinity; for example, amorphous TIPS-Pn films exhibit shifts Δ lower than 10 nm, whereas shifts of 45–70 nm were obtained in crystalline TIPS-Pn films.[37] A similar trend was obtained here in dimethylxylindein films, wherein an interplay of the absorption features of the amorphous and crystalline regions was observed in

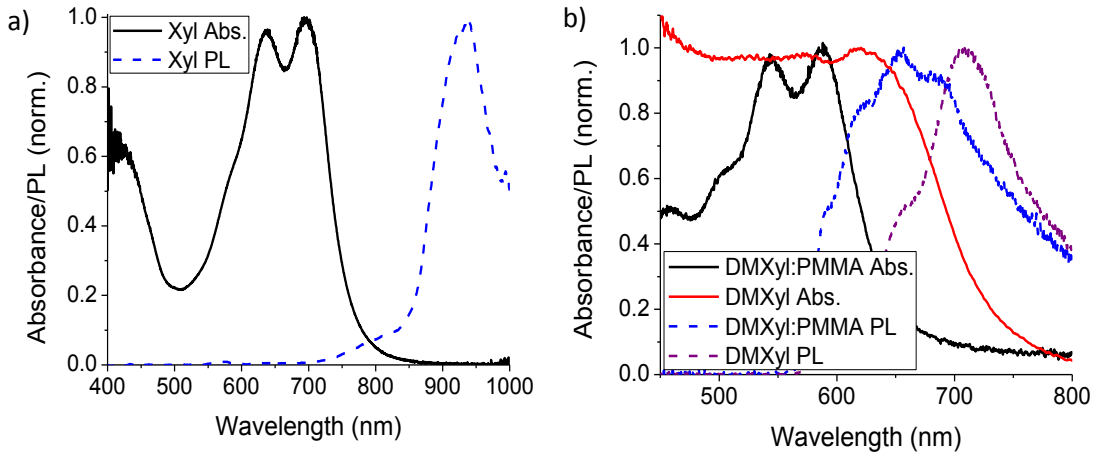

Figure 5. (a) Optical absorption and PL spectra of a xylindein film. PL was measured under 633 nm excitation. (b) Optical absorption and PL spectra of amorphous dimethylxylindein:PMMA and crystalline pristine dimethylxylindein films. PL spectra were measured under 532 nm excitation.

Table 2. Optical and (photo)conductive properties of films

	Δ, [1] nm (eV)	Abs Max,[2] nm	PL Max,[2] nm	$E_{a,PL}$[3] (eV)	μ_{eff}[4] ($cm^2/(Vs)$)	$E_{a,dark}$[5] (eV)	$E_{a,photo}$[6] (eV)
Xylindein	**42 (0.11)**	**701**	**933**	**0**	**0.05**	**0.24**	**0.18**
dimethylxylindein:PMMA	**20 (0.07)**	**591**	**649**	**0**	**1.1×10^{-6}**	**0.46**	**0.23**
Pristine dimethylxylindein	**72 (0.24)**	**643**	**713**	**0.082**	**1.1×10^{-6}**	**0.61**	**0.23**

[1]Solution-to-solid shift calculated as a difference between the absorption maximum in film and in DCM solution; in the case of xylindein, the absorption maximum (659 nm, Fig. 2a), containing contributions from both tautomers, in DCM is used. [2]Wavelength (energy) of the absorption or PL peak maximum in film. [3]Extracted from Arrhenius fit to Eq. (2) as described in text. [4]Obtained from SCLCs on coplanar Au/PEIE electrodes. [5]Obtained from Arrhenius fits to the dark currents from films on interdigitated Au/PEIE electrodes at 100 V. [6]Obtained from Arrhenius fits to the ac photocurrents from films on interdigitated Au/PEIE electrodes at 100 V under 532 nm cw excitation.

the optical absorption spectra, depending on film morphology (Fig. S9). Given that there is no crystalline order present in xylindein films, a relatively large solution-solid redshift Δ could be related to the enhanced intermolecular interactions due to intermolecular H-bonding which is absent in dimethylxylindein. A similar effect of H-bonding on Δ has been previously observed in other H-bonded pigments.[9] The redshift in the optical absorption was accompanied by a redshift in the PL emission spectra of films as compared to solutions, in both xylindein and dimethylxylindein, such that the dominant PL emission of xylindein films is at ~930 nm and that in dimethylxylindein films is at ~670–720 nm depending on morphology. The PL emission spectra from amorphous dimethylxylindein:PMMA and crystalline pristine dimethylxylindein films are shown in Fig. 5b, illustrating a redshift in the dominant emission from crystalline versus amorphous regions. Both xylindein and dimethylxylindein films exhibited short dominant PL lifetimes of <200 ps, limited by the time resolution of our PL measurements (Fig. S4 and Table S2).

Pristine dimethylxylindein films exhibit features of photodegradation under continuous 532 nm illumination in air, as shown in its PL spectral evolution (Fig. S10). No such degradation was observed in xylindein or amorphous dimethylxylindein:PMMA films, which may suggest that the mechanism of photodegradation in crystalline dimethylxylindein films relies on particular intermolecular arrangements that facilitate formation of dimers, as has been observed in, for example, crystalline acenes.[30]

Similar to solution, the Stokes shift in xylindein films (~230 nm) is considerably larger than that in dimethylxylindein-based films (~60–70 nm) (Table 2). This suggests that the ESIPT, responsible for a large Stokes shift of xylindein in solution, proceeds on ultrafast time scales in the xylindein solid form as well.

In addition to differences in the PL spectral characteristics, amorphous dimethylxylindein:PMMA and crystalline pristine dimethylxylindein films exhibited drastically different temperature dependence in the 80 – 300 K temperature range. In particular, the amorphous binary film showed weak temperature dependence in the entire temperature range studied; the same behavior was observed in xylindein films. In contrast, the PL from pristine dimethylxylindein film exhibited a strong, fully reversible, temperature dependence below ~200 K (Fig. 6). We attribute this feature to a decreased exciton diffusion at low temperatures, which inhibits nonradiative recombination, resulting in a higher QY. This can be modelled with a thermally activated nonradiative decay rate, $k_{nr}(T)$:[22]

$$k_{nr}(T) = k_{nr}^{0} + k_{nr}^{*}\, e^{-\frac{E_{a,PL}}{k_B T}} \quad (1)$$

Here, k_{nr}^{0} and k_{nr}^{*} are constants, k_B is the Boltzmann constant, and $E_{a,PL}$ is the activation energy. The PL intensity can be modelled as follows:

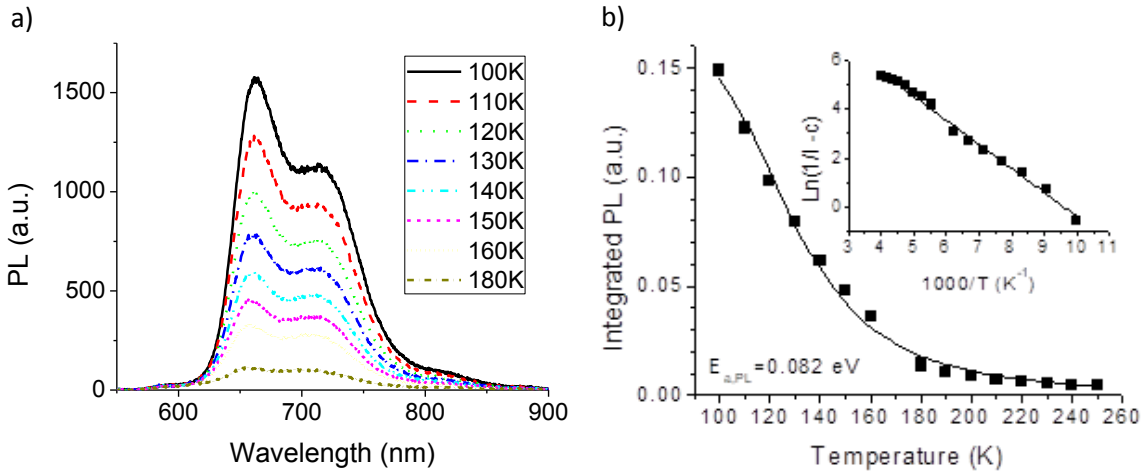

Figure 6. (a) PL spectra from a crystalline pristine dimethylxylindein thin film at temperatures below 200 K. (b) Integrated PL for crystalline dimethylxylindein film versus temperature, fit with Eq. (2). Inset shows a linearized version of the data to show quality of fit, where I is the integrated PL and c is a constant extracted from the fit related to k_{nr}^0 in Eq. (1).

$$I(T) \propto \frac{k_r}{k_r + k_{nr}(T)} \quad (2)$$

where k_r is the temperature-independent radiative rate. The integrated PL spectra (Fig. 6) were fit to Eq. (2) to extract an activation energy $E_{a,PL}$ of (82 ± 5) meV. Similar behavior has been observed in a variety of polycrystalline films,[24,38] for example those of functionalized ADT derivatives or Alq_3 with activation energies of ~69 meV[29] and ~74 meV,[39] respectively. Considerably weaker temperature dependence of PL in amorphous than crystalline films, observed in dimethylxylindein, has been previously reported in, for example, Alq_3 films.[39] This finding indicates that thermally-activated exciton diffusion to the PL quenching sites, which causes non-radiative recombination, is considerably more efficient in crystalline regions than that in amorphous regions.

3.4 Conductive and photoconductive properties

Conductive properties were investigated by measuring current-voltage (I-V) characteristics of pristine xylindein, dimethylxylindein:PMMA, and pristine dimethylxylindein films deposited on coplanar electrodes. Different electrode metals such as Au and Al, as well as different electrode treatments were investigated to optimize electrical performance, aiming to reduce contact resistance and improve matching of the work function to the free carrier energy level of the material. In our previous work,[11] xylindein films performed considerably better on Al electrodes (work function of ~4.2 eV) than the untreated Au electrodes (work function of ~5.1 eV), with effective electron mobilities of 0.1–0.4 $cm^2/(Vs)$ obtained from space-charge-limited currents (SCLCs). This is consistent with the expectations of a preferential electron transport in xylindein, supported by DFT calculations of the HOMO and LUMO energies of xylindein, which yielded −6.49 (−6.30) and −4.31 (−3.99) eV, respectively, for the two xylindein tautomers (Fig. S2 and Table 1) present in our samples. In dimethylxylindein, DFT calculations of the HOMO and LUMO orbitals (Fig. S11) yielded HOMO and LUMO energies of –6.35 eV and –3.89 eV. The low LUMO energy of dimethylxylindein suggests that similar to xylindein, dimethylxylindein should exhibit a preferential electron or ambipolar transport. In accord with these expectations, and similar to xylindein, the currents improve by a factor of 3–5 in dimethylxylindein films on Au electrodes treated with a thin layer of polyethylenimine ethoxylated (PEIE) to effectively reduce the work function (e.g. to 3.9 eV as measured by Kelvin probe in air in Ref.[23]) versus those on untreated Au electrodes (Fig. S12).

Figure 7a shows the room-temperature I-V characteristics of pristine xylindein, dimethylxylindein:PMMA, and pristine dimethylxylindein films on PEIE-treated Au electrodes. Xylindein films exhibited more than four orders of magnitude higher currents than either

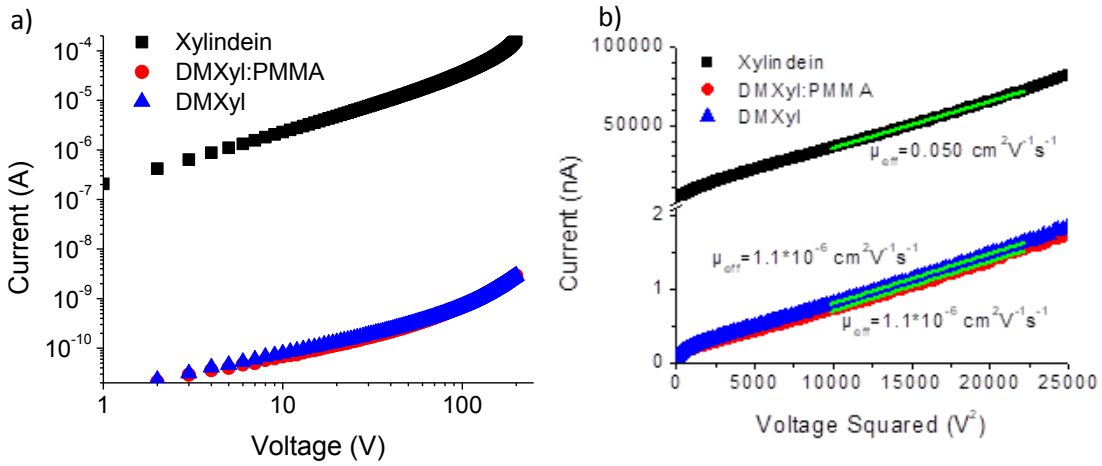

Figure 7. (a) Current-voltage characteristics for xylindein, dimethylxylindein:PMMA, and pristine dimethylxylindein (DMXyl) films. (b) Current versus voltage squared and linear fits to the data. The slope of the linear fit was used to calculate the effective SCLC mobilities, shown for the case of the infinite half-space approximation discussed in the text.

dimethylxylindein:PMMA blend or pristine dimethylxylindein films. The SCLC regime where current varies quadratically with respect to voltage[2,11] was observed in all samples at high voltages.

In the case of the planar electrode geometry used in our experiments, the current flows along a thin layer of unknown thickness, and the current density (j) is expressed in units of A/m (as opposed to A/m^2 for the "sandwich" electrode geometry). Although there is no analytical solution for the relationship between the SCLC linear current density (j) and the applied voltage (V) in a film of finite thickness on coplanar electrodes, there are solutions for the extreme cases of the infinitely thin film ("thin-film approximation") and the infinite half-space ("infinite half-space approximation").[40] In the thin-film regime, the linear current density (j) is $j = (2/\pi)\mu_{eff}\varepsilon\varepsilon_0 V^2/L^2$. Here j = I/d, where I is the measured current and d is the length of the electrode, L is the gap between the electrodes, ε_0 is the vacuum permittivity, ε is the dielectric constant (assumed here to be equal to 3), and μ_{eff} is the effective mobility. The SCLC j−V dependence in the infinite half-space approximation differs from the expression above only in the coefficient $2/\pi$, which is replaced by 0.28.[40] Our films are 3-5 μm thick, and thus for the electrode geometry with the 5 μm

gap (L) used for measurements in Fig. 7, neither the thin-film nor the half-space approximation is strictly valid and the true effective mobility lies in between the values obtained in these extreme cases. The choice of the small gap L was dictated by the need to achieve measurable currents in dimethylxylindein-based films in a wide range of applied voltages necessary to probe the transition from the linear to the SCLC regime.

Figure 7b shows current versus voltage squared for xylindein, dimethylxylindein:PMMA, and pristine dimethylxylindein films, all on PEIE-treated Au electrodes, along with linear fits from which the effective electron mobility μ_{eff} was extracted. In this geometry, xylindein exhibited effective electron mobility of ~0.022 $cm^2/(Vs)$ (0.05 $cm^2/(Vs)$) in the thin-film (half-space) approximation. These values for the effective mobilities should be considered a lower bound on actual electron mobility in these materials since trap-free SCLC regime was not achieved in either film. The effective mobility in xylindein films was more than four orders of magnitude higher than ~5×10^{-7} $cm^2/(Vs)$ (1.1×10^{-6} $cm^2/(Vs)$) obtained in both dimethylxylindein:PMMA and pristine dimethylxylindein films in the thin-film (half-space) approximation. In order to confirm that the observed drastic differences in electronic characteristics of xylindein and dimethylxylindein films are not driven by surface states, we investigated I-V characteristics of films in conventional sandwich cell geometry. In this geometry, pristine xylindein and dimethylxylindein could not be studied due to their porous and polycrystalline structure, respectively, prone to creating electrical shorts. Therefore, we employed a strategy of mixing an active small-molecule compound (in our case xylindein or dimethylxylindein) with a neutral polymer (in our case PMMA), which is a commonly used method of improving processability and electronic characteristics of organic films. Such method has been applied to a variety of small-molecule organic semiconductors, and comprehensive studies of effects of relative small-molecule:polymer concentrations, molecular

weight of the polymer, and other polymer characteristics on film morphology and device performance have been reported.[41,42] When an optimized blend is achieved, it has been shown to exhibit enhanced electronic properties as compared to those of pristine films, due to morphology-controlled improvement of charge trap characteristics.[41,43] Our previous work[12] showed that 4:1 w/w xylindein:PMMA blends had an electronic performance comparable to that of pristine xylindein films. However, sandwich cell devices of this blend experienced similar issues with electric shorts to those of pristine xylindein films. Thus, we explored xyindein:PMMA and dimethylxylindein:PMMA blends with varying concentrations, increasing the PMMA concentration until the morphology suitable for studies of electronic properties in the sandwich cell geometry was achieved. Figure S13 shows the I-V characteristics of xylindein:PMMA and dimethylxylindein:PMMA blends at 1:1 and 1:2 w/w ratios in the sandwich cell geometry, demonstrating that xylindein:PMMA films considerably outperformed dimethylxylindein:PMMA films in this geometry as well, a result similar to that obtained in pristine xylindein and dimethylxylindein devices with planar geometry in Fig. 7.

In order to explore the mechanism of conduction in films under study, temperature-dependent measurements of the I-V characteristics were carried out. Figure 8a shows temperature dependence of dark currents obtained in xylindein and dimethylxylindein films. All samples exhibited a thermally activated response ($\sim\exp[-E_{a,dark}/k_BT]$, where $E_{a,dark}$ is the activation energy, k_B is the Boltzmann constant, and T is the temperature), characteristic of thermally activated hopping of charge carriers between states exponentially distributed in energy. Dark currents in xylindein films exhibited activation energies of ~0.24 eV, similar to 0.24−0.25 eV previously obtained in blends of xylindein with PMMA or nanocellulose.[11] These activation energies are slightly lower than that of 0.3 eV obtained in pristine xylindein films on untreated substrates with Au electrodes,[11] which

is due to an improved interface morphology resulting from the PEIE treatment of the Au electrodes. The activation energies for dark currents in dimethylxylindein films were substantially higher than those for xylindein films, yielding ~0.46 and 0.61 eV in dimethylxylindein:PMMA and pristine dimethylxylindein films, respectively (Fig. 8a), indicative of the presence of deep charge traps in both dimethylxylindein-based films. The higher activation energy in the crystalline pristine dimethylxylindein films suggests that the crystallite boundaries create an additional source of deep traps. At higher temperatures, with additional thermal energy that promotes charge release from traps and enhances hopping, the difference between dark currents in xylindein and dimethylxylindein films was significantly reduced and thus, the intrinsic mobilities of these two materials are closer than Fig. 7b would suggest. However, even at 400 K (the highest temperature in our measurements) the currents in xylindein films were about a factor of ~50 higher than those in dimethylxylindein films.

The substantial difference in charge transport properties of xylindein and dimethylxylindein:PMMA films may indicate the importance of intermolecular H-bonding, discussed above in the context of optical properties, for creating molecular networks with enhanced conductive properties and reduced charge trapping. It was demonstrated[10] that intermolecular H-bonding can enhance charge transfer integrals by reducing the intermolecular distance and facilitating the electronic wave function overlap. For example, in crystalline ellipticine, similar charge carrier mobilities were obtained in the H-bonding and π–π stacking directions (4.2 $cm^2/(Vs)$ and 6.5 $cm^2/(Vs)$, respectively).[10] In amorphous xylindein and dimethylxylindein:PMMA films, although some differences are expected in the π–π stacking properties due to the bulky OMe side groups in dimethylxylindein as compared to the OH groups in xylindein, we hypothesize that the H-bonding enabled in xylindein but not in dimethylxylindein

plays a dominant role in differences between charge-transport properties of these two materials. Interestingly, in pristine dimethylxylindein films, the presence of crystalline regions did not result in higher effective charge carrier mobility than that in amorphous dimethylxylindein:PMMA films, at least in the 300—400 K temperature range studied, because of poor morphology leading to enhanced charge trapping.

Next, we examined the photoconductive properties of all films under a 532 nm and 633 nm continuous-wave excitation. Similar to dark currents, the photocurrents obtained from xylindein films were higher than those in dimethylxylindein:PMMA and pristine dimethylxylindein films, but the difference in the photocurrents was smaller than that in the dark currents. For example, at room temperature the dc photocurrents measured under the same illumination conditions excitation were about two orders of magnitude higher in xylindein than in dimethylxylindein (Fig. 8b), for both excitation wavelengths studied, as compared to about four orders of magnitude difference in dark currents in the same samples. This behavior can be understood from comparisons of the photosensitivity of xylindein and dimethylxylindein, defined as the ratio of photocurrent to dark current (inset of Fig. 8b). In particular, the photosensitivity was considerably higher in dimethylxylindein, which suggests a significantly higher charge photogeneration efficiency in this material versus xylindein. This is most likely due to the differences in the excited state dynamics of these two compounds discussed above (Fig. 3). While the exact mechanism of charge photogeneration in these films requires further investigation, it is possible that exciton interaction with defects would need to be invoked in order to overcome high Frenkel exciton

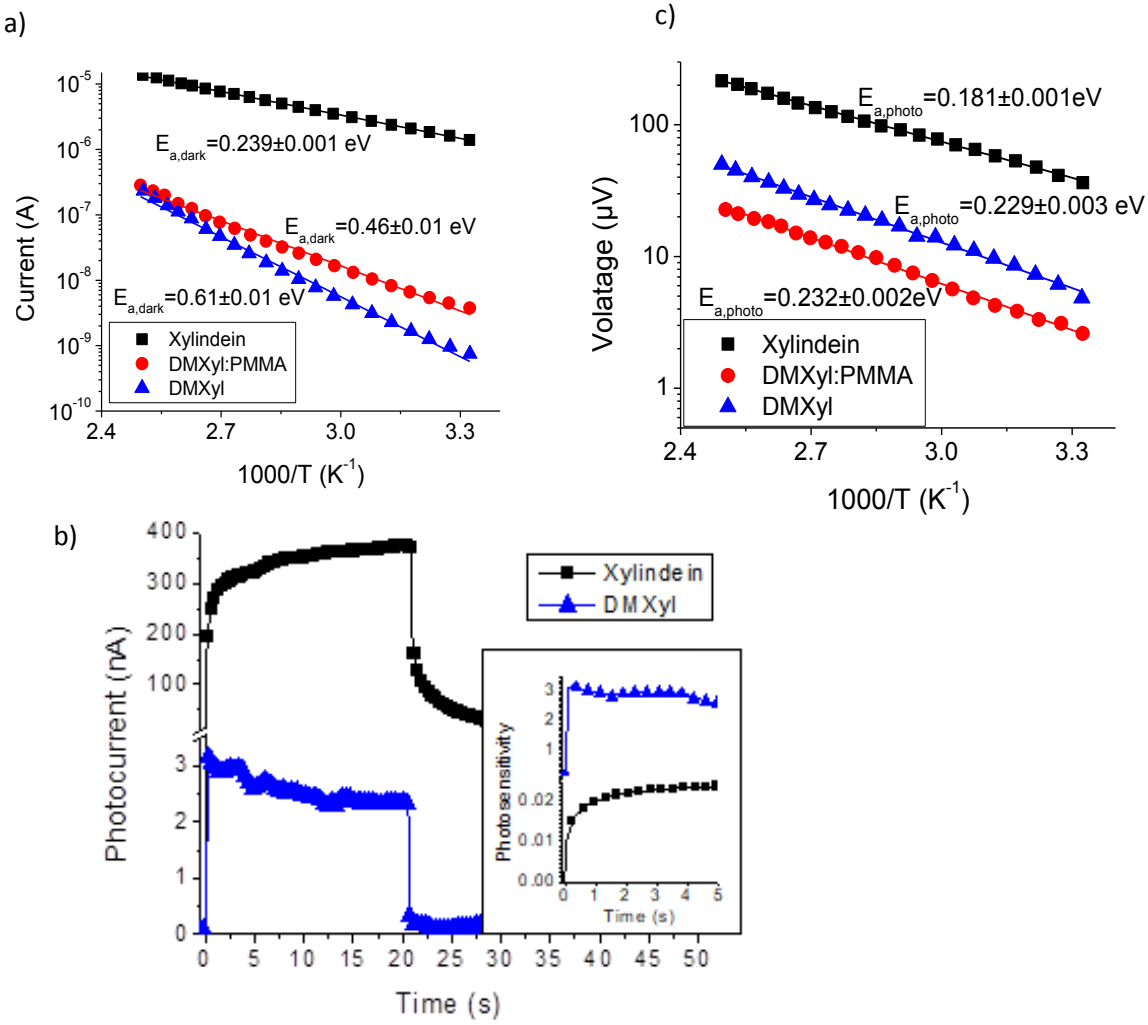

Figure 8. Temperature dependence of dark (a) and ac photo (c) currents obtained in pristine xylindein, dimethylxylindein:PMMA, and pristine dimethylxylindein (DMXyl) films. Arrhenius fits (~exp[−E_a/k_BT]) with the extracted activation energies $E_{a,\ dark}$ and $E_{a,\ photo}$ are also included. The temperature dependence was independent of the applied voltage in the range studied. (b) Photocurrent from pristine xylindein and dimethylxylindein films at 100 V under 532 nm cw laser illumination turned on at time t = 0 and off after 20 seconds. Inset shows the photosensitivity of the same films, defined as a ratio of the photocurrent to dark current.

binding energy (≳0.3 eV, Table 1). Such process would rely on exciton diffusion and depend on the exciton lifetime; for example, in rubrene crystals the charge photogeneration relies on long-range diffusion of triplet excitons to surface electron traps that promote exciton dissociation.[44] If a similar mechanism is responsible for charge photogeneration in films under study, fast depopulation of the excited state in xylindein, which is much less efficient in dimethylxylindein,

would limit the efficiency of exciton dissociation into mobile charge carriers, leading to observations in the inset of Fig. 8b.

The difference between the ac photocurrents in xylindein and dimethylxylindein films was reduced as compared to that for the dc photocurrents, from two orders of magnitude to a factor of ~10−20 at 100 Hz at room temperature (Fig. 8c). This reduction is due to the pronounced contribution of shallow traps to the photocurrents in xylindein which leads to the considerably slower photocurrent dynamics[45] in xylindein films, as compared to dimethylxylindein (Fig. 8b), and manifests into frequency-dependent photoresponse.[46]

In order to better understand the contribution of traps to the photoresponse versus dark currents, we investigated temperature dependence of the ac photocurrent in all films under study (Fig. 8c) and compared it to that of the dark currents (Fig. 8a). Similar to dark currents, the observed temperature dependence of the photocurrents could be well described by the Arrhenius function ($\sim\exp[-E_{a,photo}/k_BT]$). However, in contrast to dark currents, the activation energy for the ac photocurrents $E_{a,photo}$ was considerably lower, at ~0.18 eV for xylindein films (similar to that previously observed in xylindein:PMMA blends[11]) and ~0.23 eV for both dimethylxylindein:PMMA and pristine dimethylxylindein films. The observed $E_{a,photo}$ values, and the considerably lower activation energies for ac photocurrents as compared to dark currents are common for a variety of organic materials; for example, in an organic DCDHF glass, activation energies of 0.18 eV (0.72 eV) were obtained from the temperature dependence of photo (dark) currents.[47] The lower values of $E_{a,photo}$ as compared to $E_{a,dark}$ suggest that a considerably smaller subset of states is participating in the photoinduced charge transport sampled at millisecond time-scales as compared to that of injected carriers, and so deep charge traps contributing to the dark current in dimethylxylindein films do not contribute to the ac photocurrent.

4. CONCLUSIONS

We compared optical and (opto)electronic properties of fungi-derived pigment xylindein and its methylated derivative, dimethylxylindein via an integrated platform from wood sciences, organic synthesis, ultrafast spectroscopy, quantum chemistry calculations, to device physics. The hydroxyl groups in xylindein, which are not present in dimethylxylindein, were found to play a critical role in optical absorption and PL properties, excited state dynamics, photostability, and conductivity. Enhanced photostability of xylindein is attributed to fast deactivation of the excited state; this channel is not as efficient in dimethylxylindein with a long-lived dark (triplet) state formation being observed instead, which considerably reduces its photostability. At room temperature, amorphous xylindein films were found to be over four orders of magnitude more conductive than both amorphous and crystalline dimethylxylindein films. On the other hand, the photosensitivity of dimethylxylindein films is considerably higher than that of xylindein films, attributed to higher photogeneration efficiency in dimethylxylindein. Charge transport was thermally activated in all films under study, with the activation energies considerably lower in xylindein films as compared to dimethylxylindein films. The observed large difference in electronic properties is partly attributed to H-bonding in xylindein which promotes morphology supportive of efficient conductive network in xylindein films and reduces the average charge trap depth.

ASSOCIATED CONTENT

Supporting information

The Supporting Information is available free of charge on the ACS Publications website.

Additional optical spectral data, details of fitting procedures, PL lifetime data, XRD data, additional photodegradation data, DFT calculations, additional electronic characteristics data (PDF)

AUTHOR INFORMATION

Corresponding author

*Email: oksana@science.oregonstate.edu (O.O.)

ORCID

Oksana Ostroverkhova: 0000-0002-3833-161X

Author contributions

G.G. made samples, measured optical absorption, PL, and (photo)conductive properties, and analyzed data; T.C. and C.F. provided transient absorption data and supporting data on photostability of deprotonated form of xylindein; J.V.S. contributed DFT calculations and PL decay lifetime analysis; R.K. and C.B. synthesized dimethylxylindein; R.V.C. and S.R. provided xylindein; O.O. led the project, G.G. and O.O. wrote the manuscript; all authors edited the manuscript.

ACKNOWLEDGMENTS

We thank Prof. B. Gibbons for the access to the XRD facilities and Prof. J. E. Anthony for diF TES-ADT and TIPS-Pn. Support from the National Science Foundation grant numbers CBET-1705099 (to O.O. and S.R.) and MCB-1817949 (to C.F.) is gratefully acknowledged.

ABBREVIATIONS

ADT, anthradithiophene; CB, chlorobenzene; DCM, dichloromethane; DFT, density functional theory; ESIPT, excited-state intramolecular proton transfer; fs-TA, femtosecond transient absorption; HOMO, highest occupied molecular orbital; LUMO, lowest unoccupied molecular orbital; PEIE, polyethylenimine ethoxylated; PL, photoluminescence; PMMA, poly(methyl methacrylate); Pn, pentacene; PXX, peri-xanthenoxanthene; QY, quantum yield;

SCLC,space-charge-limited current; SCWL, supercontinuum white light; TCSPC, time correlated single-photon counting; TES, (triethylsilyl)ethynyl; TFT, thin film transistor; THF, tetrahydrofuran; TIPS, (triisopropylsilyl)ethynyl; XRD, X-ray diffraction

REFERENCES

(1) Ostroverkhova, O. Organic Optoelectronic Materials : Mechanisms and Applications. *Chem. Rev.* **2016**, *116*, 13279-13412. http://pubs.acs.org/doi/abs/10.1021/acs.chemrev.6b00127

(2) Ostroverkhova, O. *Handbook of Organic Materials for Electronic and Photonic Devices*; (Woodhead Publishing, 2019). https://doi.org/10.1016/c2016-0-05254-3.

(3) Purushothaman, B.; Parkin, S. R.; Kendrick, M. J.; David, D.; Ward, J. W.; Yu, L.; Stingelin, N.; Jurchescu, O. D.; Anthony, J. E. Synthesis and Charge Transport Studies of Stable, Soluble Hexacenes. *Chem. Commun.* **2012**, *48* (66), 8261–8263. https://doi.org/10.1039/c2cc33919f.

(4) Shepherd, W. E. B.; Grollman, R.; Robertson, A.; Paudel, K.; Hallani, R.; Loth, M. A.; Anthony, J. E.; Ostroverkhova, O. Single-Molecule Imaging of Organic Semiconductors: Toward Nanoscale Insights into Photophysics and Molecular Packing. *Chem. Phys. Lett.* **2015**, *629*, 29–35. https://doi.org/10.1016/j.cplett.2015.04.014.

(5) Grollman, R.; Quist, N.; Robertson, A.; Rath, J.; Purushothaman, B.; Haley, M. M.; Anthony, J. E.; Ostroverkhova, O. Single-Molecule Level Insight into Nanoscale Environment-Dependent Photophysics in Blends. *J. Phys. Chem. C* **2017**, *121* (22), 12483–12494. https://doi.org/10.1021/acs.jpcc.7b03729.

(6) Zhang, L.; Fonari, A.; Liu, Y.; Hoyt, A. L. M.; Lee, H.; Granger, D.; Parkin, S.; Russell, T. P.; Anthony, J. E.; Brédas, J. L., et al. Bistetracene: An Air-Stable, High-Mobility

Organic Semiconductor with Extended Conjugation. *J. Am. Chem. Soc.* **2014**, *136* (26), 9248–9251. https://doi.org/10.1021/ja503643s.

(7) Irimia-Vladu, M.; Glowacki, E. D.; Sariciftci, N. S.; Bauer, S. Natural Materials for Organic Electronics. In *Small Organic Molecules on Surfaces*; 2013; Vol. 173, pp 295–318. https://doi.org/10.1007/978-3-642-33848-9.

(8) Głowacki, E. D.; Voss, G.; Leonat, L.; Irimia-Vladu, M.; Bauer, S.; Sariciftci, N. S. Indigo and Tyrian Purple - From Ancient Natural Dyes to Modern Organic Semiconductors. *Israel Journal of Chemistry*. John Wiley & Sons, Ltd., 2012, pp 540–551. https://doi.org/10.1002/ijch.201100130.

(9) Głowacki, E. D.; Irimia-Vladu, M.; Kaltenbrunner, M.; Gasiorowski, J.; White, M. S.; Monkowius, U.; Romanazzi, G.; Suranna, G. P.; Mastrorilli, P.; Sekitani, T., et al. Hydrogen-Bonded Semiconducting Pigments for Air-Stable Field-Effect Transistors. *Adv. Mater.* **2013**, *25* (11), 1563–1569. https://doi.org/10.1002/adma.201204039.

(10) Zhang, F.; Lemaur, V.; Choi, W.; Kafle, P.; Seki, S.; Cornil, J.; Beljonne, D.; Diao, Y. Repurposing DNA-Binding Agents as H-Bonded Organic Semiconductors. *Nat. Commun.* **2019**, *10* (1), 1–11. https://doi.org/10.1038/s41467-019-12248-9.

(11) Giesbers, G.; Van Schenck, J.; Quinn, A.; Van Court, R.; Vega Gutierrez, S. M.; Robinson, S. C.; Ostroverkhova, O. Xylindein: Naturally Produced Fungal Compound for Sustainable (Opto)Electronics. *ACS Omega* **2019**, *4* (8), 13309–13318. https://doi.org/10.1021/acsomega.9b01490.

(12) Giesbers, G.; Van Schenck, J.; Vega Gutierrez, S.; Robinson, S.; Ostroverkhova, O. Fungi-Derived Pigments for Sustainable Organic (Opto)Electronics. In *MRS Advances*; **2018**; *3*, 3459–3464. https://doi.org/10.1557/adv.2018.446.

(13) Giesbers, G.; Krueger, T.; Van Schenck, J.; Van Court, R.; Morré, J.; Fang, C.; Robinson, S.; Ostroverkhova, O. Fungi-Derived Xylindein: Effect of Purity on Optical and Electronic Properties. *MRS Adv.* **2019**, *4* (31–32), 1769–1777. https://doi.org/10.1557/adv.2019.269.

(14) Robinson, S. Decay, Discovery, and Artistry – A Journey. *Am. Sci.* **2014**, *102* (3), 206–213.

(15) Robinson, S. C.; Michaelsen, H.; Robinson, J. C. *Spalted Wood: The History, Science, and Art of a Unique Material*; Schiffer Publishing: Atglen, Pennsylvania, 2016.

(16) Al-Aqar, R.; Benniston, A. C.; Harriman, A.; Perks, T. Structural Dynamics and Barrier Crossing Observed for a Fluorescent O-Doped Polycyclic Aromatic Hydrocarbon. *ChemPhotoChem* **2017**, *1* (5), 198–205. https://doi.org/10.1002/cptc.201600016.

(17) Sciutto, A.; Berezin, A.; Lo Cicero, M.; Miletić, T.; Stopin, A.; Bonifazi, D. Tailored Synthesis of N -Substituted Peri-Xanthenoxanthene Diimide (PXXDI) and Monoimide (PXXMI) Scaffolds. *J. Org. Chem.* **2018**, *83* (22), 13787–13798. https://doi.org/10.1021/acs.joc.8b02076.

(18) Christensen, J. A.; Zhang, J.; Zhou, J.; Nelson, J. N.; Wasielewski, M. R. Near-Infrared Excitation of the Peri-Xanthenoxanthene Radical Cation Drives Energy-Demanding Hole Transfer Reactions. *J. Phys. Chem. C* **2018**, *122* (41), 23364–23370. https://doi.org/10.1021/acs.jpcc.8b07819.

(19) Kobayashi, N.; Sasaki, M.; Nomoto, K. Stable Peri-Xanthenoxanthene Thin-Film Transistors with Efficient Carrier Injection. *Chem. Mater.* **2009**, *21* (3), 552–556. https://doi.org/10.1021/cm802826m.

(20) Lv, N.; Xie, M.; Gu, W.; Ruan, H.; Qiu, S.; Zhou, C.; Cui, Z. Synthesis, Properties, and

Structures of Functionalized Peri -Xanthenoxanthene. *Org. Lett.* **2013**, *15* (10), 2382–2385. https://doi.org/10.1021/ol400790d.

(21) Wang, L.; Duan, G.; Ji, Y.; Zhang, H. Electronic and Charge Transport Properties of Peri-Xanthenoxanthene: The Effects of Heteroatoms and Phenyl Substitutions. *J. Phys. Chem. C* **2012**, *116* (43), 22679–22686. https://doi.org/10.1021/jp306326e.

(22) Saikawa, Y.; Watanabe, T.; Hashimoto, K.; Nakata, M. Absolute Configuration and Tautomeric Structure of Xylindein, a Blue-Green Pigment of Chlorociboria Species. *Phytochemistry* **2000**, *55* (3), 237–240. https://doi.org/10.1016/S0031-9422(00)00282-X.

(23) Zhou, Y.; Fuentes-Hernandez, C.; Shim, J.; Meyer, J.; Giordano, A. J.; Li, H.; Winget, P.; Papadopoulos, T.; Cheun, H.; Kim, J., et al. Universal Method to Produce Low-Work Function Electrodes for Organic Electronics. *Science* **2012**, *336* (6079), 327–332. https://doi.org/10.1126/science.1218829.

(24) Platt, A. D.; Day, J.; Subramanian, S.; Anthony, J. E.; Ostroverkhova, O. Optical, Fluorescent, and (Photo)Conductive Properties of High-Performance Functionalized Pentacene and Anthradithiophene Derivatives. *J. Phys. Chem. C* **2009**, *113* (31), 14006–14014. https://doi.org/10.1021/jp904021p.

(25) Tang, L.; Zhu, L.; Taylor, M. A.; Wang, Y.; James Remington, S.; Fang, C. Excited State Structural Evolution of a GFP Single-Site Mutant Tracked by Tunable Femtosecond-Stimulated Raman Spectroscopy. *Molecules* **2018**, *23* (9). https://doi.org/10.3390/molecules23092226.

(26) Taylor, M. A.; Zhu, L.; Rozanov, N. D.; Stout, K. T.; Chen, C.; Fang, C. Delayed Vibrational Modulation of the Solvated GFP Chromophore into a Conical Intersection. *Phys. Chem. Chem. Phys.* **2019**, *21* (19), 9728–9739. https://doi.org/10.1039/c9cp01077g.

(27) Liebel, M.; Schnedermann, C.; Wende, T.; Kukura, P. Principles and Applications of Broadband Impulsive Vibrational Spectroscopy. *J. Phys. Chem. A* **2015**, *119* (36), 9506–9517. https://doi.org/10.1021/acs.jpca.5b05948.

(28) Liu, W.; Wang, Y.; Tang, L.; Oscar, B. G.; Zhu, L.; Fang, C. Panoramic Portrait of Primary Molecular Events Preceding Excited State Proton Transfer in Water. *Chem. Sci.* **2016**, *7* (8), 5484–5494. https://doi.org/10.1039/c6sc00672h.

(29) Platt, A.; Kendrick, M.; Loth, M.; Anthony, J.; Ostroverkhova, O. Temperature Dependence of Exciton and Charge Carrier Dynamics in Organic Thin Films. *Phys. Rev. B* **2011**, *84* (23), 235209. https://doi.org/10.1103/PhysRevB.84.235209.

(30) Spano, F. C. The Spectral Signatures of Frenkel Polarons in H-and J-Aggregates. *Acc. Chem. Res.* **2009**, *43* (3), 429–439. https://doi.org/10.1021/ar900233v.

(31) Krueger, T. D.; Giesbers, G.; Van Court, R.; Zhu, L.; Kim, R.; Beaudry, C. M.; Robinson, S. C.; Ostroverkhova, O.; Fang, C. Ultrafast Dynamics and Photoresponse of a Fungi-Derived Pigment Xylindein from Solution to Thin Films. *Chem. - A Eur. J.* **2021**, in press. https://doi.org/10.1002/chem.202005155

(32) Fang, C.; Tang, L.; Oscar, B. G.; Chen, C. Capturing Structural Snapshots during Photochemical Reactions with Ultrafast Raman Spectroscopy: From Materials Transformation to Biosensor Responses. *J. Phys. Chem. Lett.* **2018**, 3253–3263. https://doi.org/10.1021/acs.jpclett.8b00373.

(33) Tang, L.; Wang, Y.; Zhu, L.; Lee, C.; Fang, C. Correlated Molecular Structural Motions for Photoprotection after Deep-UV Irradiation. *J. Phys. Chem. Lett.* **2018**, *9* (9), 2311–2319. https://doi.org/10.1021/acs.jpclett.8b00999.

(34) Yamazaki, S.; Sobolewski, A. L.; Domcke, W. Molecular Mechanisms of the

Photostability of Indigo. *Phys. Chem. Chem. Phys.* **2011**, *13* (4), 1618–1628. https://doi.org/10.1039/c0cp01901a.

(35) Tan, J.; Garakyaraghi, S.; Tagami, K.; Frano, K.; Crockett, H.; Ogata, A.; Patterson, J.; Wustholz, K. Contributions from Excited-State Proton and Electron Transfer to the Blinking and Photobleaching Dynamics of Alizarin and Purpurin. *J. Phys. Chem. C* **2017**, 121, 97-106.

(36) Fudickar, W.; Linker, T. Why Triple Bonds Protect Acenes from Oxidation and Decomposition. *J. Am. Chem. Soc.* **2012**, *134* (36), 15071–15082. https://doi.org/10.1021/ja306056x.

(37) Ostroverkhova, O.; Shcherbyna, S.; Cooke, D. G.; Egerton, R. F.; Hegmann, F. A.; Tykwinski, R. R.; Parkin, S. R.; Anthony, J. E. Optical and Transient Photoconductive Properties of Pentacene and Functionalized Pentacene Thin Films: Dependence on Film Morphology. *J. Appl. Phys.* **2005**, *98* (3), 033701. https://doi.org/10.1063/1.1949711.

(38) Panzer, F.; Sommer, M.; Bässler, H.; Thelakkat, M.; Köhler, A. Spectroscopic Signature of Two Distinct H-Aggregate Species in Poly(3-Hexylthiophene). *Macromolecules* **2015**, *48* (5), 1543–1553. https://doi.org/10.1021/acs.macromol.5b00129.

(39) Ravi Kishore, V. V. N.; Narasimhan, K. L.; Periasamy, N. On the Radiative Lifetime, Quantum Yield and Fluorescence Decay of Alq in Thin Films. *Phys. Chem. Chem. Phys.* **2003**, *5* (7), 1386–1391. https://doi.org/10.1039/b211264g.

(40) Day, J.; Platt, A. D.; Subramanian, S.; Anthony, J. E.; Ostroverkhova, O. Influence of Organic Semiconductor-Metal Interfaces on the Photoresponse of Functionalized Anthradithiophene Thin Films. *J. Appl. Phys.* **2009**, *105* (10), 103703. https://doi.org/10.1063/1.3129693.

(41) Niazi, M.; Li, R.; Li E. Q.; Kirmani, A.; Abdelsamie, M.; Wang, Q.; Pan, W.; Payne, M.; Anthony, J. E.; Smilgies, D., et al. Solution-printed Organic Semiconductor Blends Exhibiting Transport Properties on par with Single Crystals. *Nat. Comm*. **2015**, 6, 8598.

(42) Lee, W.; Park, Y. Organic Semiconductor/insulator Polymer Blends for High-performance Organic Transistors. *Polymers* **2014**, 6, 1057-1063.

(43) Hunter, S.; Chen, J.; Anthopoulos, T. Microstructural Control of Charge Transport in Organic Blend Thin-film Transistors. *Advanced Functional Materials* **2014**, 24, 5969-5976.

(44) Bruevich, V.; Choi, H. H.; Podzorov, V. The Photo-Hall Effect in High-Mobility Organic Semiconductors. *Adv. Funct. Mater.* **2020**, 2006178 https://doi.org/10.1002/adfm.202006178.

(45) Paudel, K.; Johnson, B.; Neunzert, A.; Thieme, M.; Purushothaman, B.; Payne, M. M.; Anthony, J. E.; Ostroverkhova, O. Small-Molecule Bulk Heterojunctions: Distinguishing between Effects of Energy Offsets and Molecular Packing on Optoelectronic Properties. *J. Phys. Chem. C* **2013**, *117* (47), 24752–24760. https://doi.org/10.1021/jp4093089.

(46) Day, J., Subramanian, S., Anthony, J. E., Lu, Z., Twieg, R. J., Ostroverkhova, O. Photoconductivity in organic thin films: from picoseconds to seconds after excitation. *J. Appl. Phys.* **103**, 123715 (2008).

(47) Ostroverkhova, O.; He, M.; Twieg, R. J.; Moerner, W. E. Role of Temperature in Controlling Performance of Photorefractive Organic Glasses. *ChemPhysChem* **2003**, *4* (7), 732–744. https://doi.org/10.1002/cphc.200200633.

TOC Graphic